Structure controlled long-range sequential tunneling in carbon-based molecular junctions

Morteza Najarian, Amin; Mccreery, Richard L.

National Research Council Canada

Conseil national de recherches Canada

Structure Controlled Long-Range Sequential Tunneling in Carbon-Based Molecular Junctions
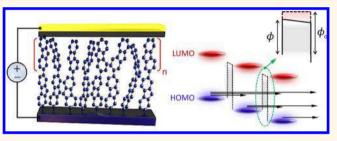
Amin Morteza Najarian[†,‡][ID] and Richard L. McCreery*[,†,‡][ID]

[†]Department of Chemistry, University of Alberta, Edmonton, Alberta T6G 2R3, Canada
[‡]National Institute for Nanotechnology, National Research Council Canada, Ottawa, Ontario T6G 2G2, Canada

Ⓢ *Supporting Information*

ABSTRACT: Carbon-based molecular junctions consisting of aromatic oligomers between conducting sp^2 hybridized carbon electrodes exhibit structure-dependent current densities (J) when the molecular layer thickness (d) exceeds ~5 nm. All four of the molecular structures examined exhibit an unusual, nonlinear ln J vs bias voltage (V) dependence which is not expected for conventional coherent tunneling or activated hopping mechanisms. All molecules exhibit a weak temperature dependence, with J increasing typically by a factor of 2 over the range of 200−440 K. Fluorene and anthraquinone show linear plots of ln J vs d with nearly identical J values for the range $d = 3−10$ nm, despite significant differences in their free-molecule orbital energy levels. The observed current densities for anthraquinone, fluorene, nitroazobenzene, and bis-thienyl benzene for $d = 7−10$ nm show no correlation with occupied (HOMO) or unoccupied (LUMO) molecular orbital energies, contrary to expectations for transport mechanisms based on the offset between orbital energies and the electrode Fermi level. UV−vis absorption spectroscopy of molecular layers bonded to carbon electrodes revealed internal energy levels of the chemisorbed films and also indicated limited delocalization in the film interior. The observed current densities correlate well with the observed UV−vis absorption maxima for the molecular layers, implying a transport mechanism determined by the HOMO−LUMO energy gap. We conclude that transport in carbon-based aromatic molecular junctions is consistent with multistep tunneling through a barrier defined by the HOMO−LUMO gap, and not by charge transport at the electrode interfaces. In effect, interfacial "injection" at the molecule/electrode interfaces is not rate limiting due to relatively strong electronic coupling, and transport is controlled by the "bulk" properties of the molecular layer interior.

KEYWORDS: molecular electronics, charge transport, multistep tunneling, thermally assisted tunneling, electronic coupling, localization length

The field of molecular electronics (ME) investigates charge transport in single molecules or ensembles of molecules oriented between conducting contacts acting as elements in electronic circuits. A core principle in ME is the control of charge transport by variations in molecular structure and the possibly wide variety of electronic functions which may be available with molecular components but difficult with conventional semiconductors. Numerous experimental paradigms have been employed in extensive research on how structure controls transport, in alkane, aromatic, and oligomeric molecular junctions (MJs).[1−5] A key parameter in charge transport is the length of the molecular component (d, in nm) between conducting contacts, and the dependence of MJ current on d is often a useful diagnostic for transport mechanism. For example, the exponential dependence of current density, J (A/cm²), at a given bias voltage on d is often cited as an indication of quantum mechanical tunneling, with the slope of ln J vs d yielding $β$, the attenuation coefficient with units of Å⁻¹ or nm⁻¹.[6] From transport measurements in donor−acceptor complexes, modified electrodes, and MJs of both single molecules and ensembles, $β$ is generally accepted to equal 6−9 nm⁻¹ for aliphatic molecules,[7−11] while $β$ is in the range of 2−5 nm⁻¹ for conjugated or aromatic molecules[12−15] and <1 nm⁻¹ for certain metal complexes with strong electronic coupling between molecular subunits.[16−18] Carbon-based MJs with carbon/molecule/Cu or carbon/molecule/carbon structures containing aromatic molecular layers exhibit $β$ values of ~2.1−3.3 nm⁻¹ and a weak dependence on variations in structure for $d < 5$ nm due to strong electronic coupling between the molecules and contacts.[13,15,19]
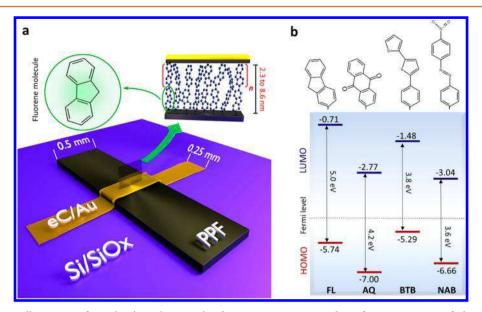
Figure 1. (a) Schematic illustration of PPF/FL/eC$_{10}$/Au$_{20}$ molecular junction; n is a number of repeating units of oligomer that determines final thickness of molecular layer. (b) Structures and frontier orbital energy diagram for FL, AQ, NAB, and BTB, relative to a vacuum reference. Orbital energies were calculated by DFT B3LYP 6-31G(d), in Gaussian 09. Fermi level of PPF and eC is −4.8 V vs vacuum.

Plots of ln J vs d for conjugated and aromatic MJs are often reported to extend from $d < 1$ nm to $d = 5$ nm, depending on molecular structure and experimental paradigm. For example, oligomers of phenyleneimines exhibit $\beta = 3.0$ nm^{-1} for $d < 4$ nm, then a change in slope to $\beta = 0.9$ nm^{-1} for $d = 4$ to 7.5 nm.[20,21] A similar change in slope was reported for oligophenylethynyl molecules, with $\beta = 0.9$ nm^{-1} for $d = 1$ to 2.5 nm and $\beta = 0.3$ nm^{-1} for $d = 2.5$ to 5.1 nm.[22] In several cases, the change in slope was attributed to a change in mechanism from direct or coherent tunneling to "hopping" involving a series of steps between sites in the molecular layer.[23,24] For bis-thienyl benzene (BTB) oligomers in carbon-based MJs, linearity of the attenuation plot with $\beta = 2.9$ nm^{-1} was observed for $d = 2-8$ nm, then $\beta = 1.0$ nm^{-1} for $d = 8-16$ nm and $\beta \approx 0.02$ nm^{-1} for 16−22 nm. For BTB, the 1.0 nm^{-1} region extended from $d = 8$ to 22 nm at low temperature, thus ruling out activated redox exchange.[25] The general consensus to date associates the linear $\beta \sim 3$ nm^{-1} region for conjugated molecules to direct tunneling, with a barrier determined by the offset between the electrode Fermi level and the molecular orbital closest in energy. Such transport may involve "electron tunneling" mediated by the molecular LUMO or "hole tunneling" mediated by the HOMO and is often referred to as the "single level model".[26,27] For transport distances above 3−5 nm in conjugated molecules, several alternatives to coherent tunneling have been proposed, including redox exchange,[21,28] polaron tunneling,[29] and field ionization,[25] although coherent tunneling remains a possibility.[17] The dependence of junction current on temperature, thickness, and bias is valuable for determining transport mechanism, and each mechanism may be affected by molecular structure quite differently.

Our laboratory has studied carbon-based MJs containing aromatic oligomers covalently bonded to conducting carbon surfaces, with Cu or carbon/Au top contacts. For molecular layer thicknesses in the range of 2−5 nm, transport has the characteristics of coherent tunneling, with weak temperature dependence and linear attenuation plots with $\beta = 2.7 \pm 0.6$ nm^{-1} for seven different aromatic structures and >400 MJs.[15]

However, both β and current density were very similar for aromatic structures, despite a variation of >2.3 eV in the HOMO and LUMO levels of the free molecules. We attributed this result to strong electronic coupling between the molecules and the contacts, which reduces the influence of electron-donating or -withdrawing groups on the observed transport barrier. Strong coupling between graphitic electrodes and aromatic molecules is also predicted theoretically, leading to significant shifts in HOMO and LUMO levels in graphene-molecule model structures relative to those of the free molecules.[30−32] The current investigation was undertaken to address two questions about transport through organic films with thicknesses >5 nm. First, how far does the exponential dependence on layer thickness extend past 5 nm; and second, what transport mechanisms become operative once coherent tunneling becomes negligible? Three aromatic molecular layers that could be extended to thicknesses >5 nm were examined and compared to past results for a thiophene derivative in the same thickness range. A detailed analysis of the current−voltage response of diazonium-derived fluorene oligomers between carbon contacts and $d = 2.3$ to 8.6 nm revealed an unexpected behavior which is inconsistent with either coherent tunneling or the "single level" model commonly applied to aromatic MJs. Comparison to anthraquinone (AQ) and nitroazobenzene (NAB) MJs permitted insights into the factors controlling charge transport, and a multistep tunneling mechanism explains the experimental results.

RESULTS

Fluorene (FL) molecular junctions with thicknesses (d) of 2.3−8.6 nm were examined in detail initially in order to characterize transport for molecular layers with $d > 5$ nm. Figure 1a shows a junction schematic and cross section of a completed device as well as the structure of FL and its oligomer. After describing their JV behavior, temperature dependence, and UV−vis absorption, additional MJs containing NAB, AQ, and BTB were examined for comparison, before proposing a transport mechanism. Figure 1b shows the four aromatic molecules used in the current work, with the density functional theory (DFT)-
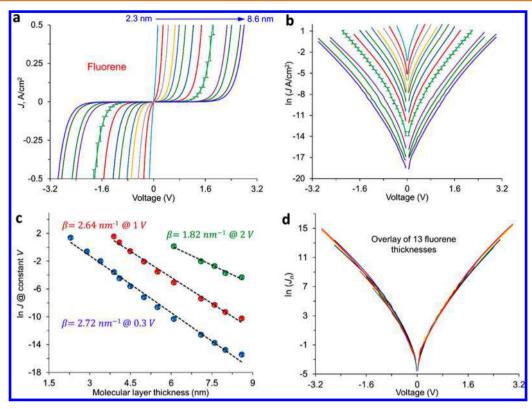
Figure 2. (a) Current density vs bias voltage (JV) curves for PPF/FL$_d$/eC$_{10}$/Au$_{20}$; d is a thickness of FL molecular layer: d = 2.3, 3.0, 3.4, 3.8, 4.1, 4.5, 5.0, 5.5, 6.1, 7.1, 7.6, 8.0, 8.6 nm in the order indicated. Each curve is an average of four independent junctions, with a typpical deviation shown for d = 6.1 nm junction. (b) Semilogarithmic plot of JV curves shown in panel a. (c) Corresponding attenuation plot for V = 0.3, 1.0, and 2.0 V, with the slopes (β) indicated. (d) Overlay of normalized semilogarithmic JV curves shown in panel b. Current density of each thickness was normalized to J = 1 A/cm^2 at 0.3 V.

predicted energy levels of the free molecules relative to the vacuum level.

Fluorene JV Behavior. Current density vs bias voltage (JV) curves for FL MJs with 13 thicknesses in the range of 2.3−8.6 nm are shown in Figure 2a. Error bars on the response for 6.1 nm thickness indicate typical standard deviations of J, and all curves are averages of four separate MJs. Additional statistics and sample JV curves are available in Supporting Information (SI) section 2 and Figure S5. The same results are shown in semilog format in Figure 2b, with error bars shown for the 6.1 nm case. Comparison of the JV curves clearly illustrates that (i) junction conductance depends nonlinearly on bias; (ii) JV curves are nearly symmetric with respect to bias polarity for all thicknesses; and (iii) there is a strong thickness dependence of conductivity, with conductance decreasing monotonically with thickness at all bias values. Note also that the ln J vs V curves do not exhibit the linearity expected for direct tunneling, and this point will be discussed in more detail below. Attenuation plots of ln J vs junction thickness (d) are shown in Figure 2c, for three bias values. For V = 0.3 V, β = 2.72 nm^{-1}, in good agreement with that reported previously for seven other diazonium-derived aromatic junctions (β = 2.7 $\pm$ 0.6 nm^{-1})[15] and β = 2.9 nm^{-1} for BTB devices with d < 8 nm.[25] Note particularly that the exponential decrease in current density for FL devices extends well beyond the usual limit for direct tunneling of 3−5 nm, with minor changes in slope over the entire 2.3−8.6 nm range. A further test of the similarity of the JV response for different thicknesses is an overlay of the JV curves after normalization of the currents for all curves at V = 0.3 V to J = 1 A/cm^2, as shown in Figure 2d. The 13 curve

shapes are very similar over the entire voltage range, implying that the J vs V behavior for all thicknesses has similar shape and dependence on bias.

As noted above, the nonlinearity of the ln J vs V plots in Figure 2b is not expected for direct tunneling, and other transport mechanisms can result in such curvature. Poole−Frenkel transport between Coulombic traps and Schottky emission at interfaces can both predict linearity of ln J with $V^{1/2}$, due to changes in the respective barriers with increases in electric field.[33] We considered these mechanisms previously for BTB devices in the thickness range of 8−12 nm, but rejected them due to inconsistency with the temperature dependence of the JV curves.[25] Figure 3 shows ln J vs $V^{1/2}$ plots for comparison to ln J vs V in Figure 2b, and statistics for linear fits of ln J to V, ln J to $V^{1/2}$, ln J/V to $V^{1/2}$ and other possible functional forms are listed in Supporting Information section 3 and Table S2. For d = 2.3−6.1 nm, the ln J vs $V^{1/2}$ plots are very linear, with R^2 above 0.997 in all cases, while R^2 for the ln J vs V plots ranges from 0.973 to 0.985. Slight upward curvature of the ln J vs $V^{1/2}$ plots is observed for d = 7.1 to 8.6 nm, but still results in a better linear fit (R^2 > 0.994 for d = 8.6 nm) than either ln J vs V (R^2 > 0.985) or ln J/V vs $V^{1/2}$ (R^2 = 0.981). The slopes, intercepts, and R^2 values for linear fits of ln J vs $V^{1/2}$ plots of all 13 FL thicknesses are provided in Table S3.

Fluorene Temperature Dependence. We reported previously that BTB molecular junctions with d > 16 nm exhibited Arrhenius temperature dependence with E_{act} > 100 meV above 200 K, but thinner molecular layers and T < 200 T had apparent Arrhenius slopes in the range of 0−50 meV.[25] We also reported that aromatic MJs with d < 5 nm had a weak
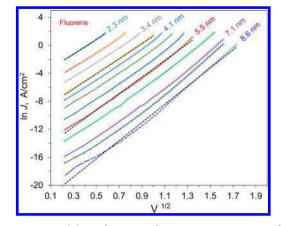
Figure 3. Natural log of current density *vs* square root of bias voltage for the same series of FL junctions shown in Figure 2, for positive bias. Order of thickness is the same as in Figure 2a.

temperature-dependent *JV* response, consistent with coherent tunneling with the addition of Fermi function broadening for T > 200 K.[13] Tunneling in single porphyrin oligomers over a distance to 5−10 nm exhibited Arrhenius slopes of 80−220 meV, but were concluded to be inconsistent with a hopping model.[17] The *JV* curves for FL devices with d = 5.5 nm shown in Figure 4a exhibit a weak dependence on temperature with J at 440 K less than twice that of J at 200 K. Plots of ln J *vs* $V^{1/2}$ remain linear from 200 to 440 K (Figure 4b). The Arrhenius plots of Figure 4c for two bias values show no linear regions, with a significant change in slope over the observed T range. Although these results are inconsistent with Arrhenius behavior, apparent activation energies (E_{act}) are provided over limited temperature ranges in Figure 4c and Table S4. For d = 5.5 nm

at V = 0.1 V, the apparent Arrhenius slopes are 8 meV in the 200−220 K range, 51 meV for 300−320 K, and 133 meV for 420−440 K. We found that the plots of ln J *vs* T shown in Figure 4d are more linear than the Arrhenius format, with R^2 > 0.97 compared to <0.89 for Figure 4c. This fact remains valid for other measured thicknesses, and corresponding plots are provided in Figures S11 and S12. The linearity of ln J *vs* T from 240 to 440 K still indicates a temperature-dependent mechanism in this range, but clearly not classical Arrhenius behavior.

The temperature dependence of BTB was reported for a range of thicknesses previously[25] and is qualitatively similar to that of FL, with low apparent activation energies and curved Arrhenius plots. If the same BTB data are replotted as ln J *vs* T, linearity is observed for 8.1 and 10.4 nm, shown in Figure S14. AQ exhibits linearity of ln J *vs* T for four thicknesses (Figure S14), and NAB shows apparent Arrhenius slopes of <50 meV for d = 3.5, 8.0, and 35 nm.[34]

Optical Absorption by Molecular Layers. A direct indication of molecular orbital energies in the molecular layer is provided by the UV−vis absorption spectrum of FL bonded to optically transparent PPF (OTPPF) .[35−37] Here, we use UV−vis absorption to gain insight into electronic coupling within the molecular layer and between the molecules and the contacts. Figure 5a shows a UV−vis spectrum of FL monomer in acetonitrile, compared to that of a diazonium-derived FL molecular multilayer grafted on the surface of OTPPF. In the latter case, a spectrum of unmodified PPF was subtracted to reveal the molecular layer spectrum (as described in Supporting Information section 4).

There is a small (6 nm) red shift in the peak absorption wavelength upon FL bonding to PPF, but also an ~80 nm red
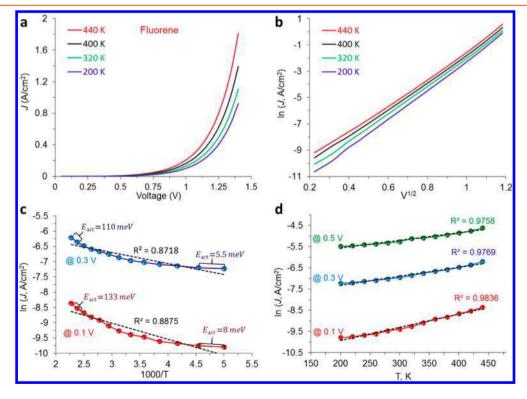

Figure 4. (a) *JV* curves for PPF/FL$_{5.5}$/eC$_{10}$/Au$_{20}$ junction at four temperatures from 200 to 440 K in vacuum. (b) ln J *vs* $V^{1/2}$ plots for curves in panel a. (c) Arrhenius plots at 0.1 and 0.3 V, with apparent activation energies for high and low T segments. (d) ln J *vs* T at 0.1, 0.3, and 0.5 V. R^2 for linear fits of the lines are indicated.
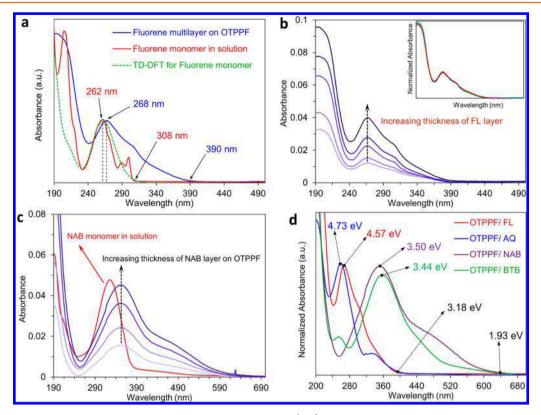
Figure 5. (a) Optical absorbance spectrum of FL monomer in acetonitrile (red) and FL multilayer bonded to the surface of OTPPF (blue), after subtraction of unmodified OTPPF spectrum. TD-DFT prediction of FL monomer spectrum is dashed green line. (b) Optical absorbance of four thicknesses of FL on OTPPF in the range of ~2−9 nm. Inset: normalized spectra for different FL thicknesses. (c) Absorbance spectra of increasing thicknesses of NAB bonded to PPF, with that of NAB monomer in ACN for comparison (red). (d) Absorbance spectra for FL, AQ, NAB, and BTB multilayers bonded to OTPPF, all following subtraction of unmodified OTPPF spectrum.

shift in the onset of the absorbance at 390 nm. At least some of this shift is due to electronic coupling[30−32] between the FL and the OTPPF and was reported previously for OTPPF/ nitroazobenzene bonded to OTPPF.[36] Figure 5b shows the absorption spectra of four films of FL on OTPPF with thicknesses increasing from ~2 to 9 nm, as indicated. The onset of absorbance at 390 nm does *not* change with increasing thickness, and the normalized spectra in the inset show that the entire spectrum shape is unchanged with thickness. Several authors have discussed a "localization length"[38] or "effective conjugation length"[39] as the oligomer length where additional subunits no longer change the absorption spectrum.[16,17,29,40] Tsuda *et al.*[39] reported that the localization length can extend to more than 12 fused coplanar porphyrin units with 175 nm red shift per subunit. However, the localization length in nonfused aromatic oligomers can be decreased by the nonzero dihedral angles of neighboring units and disordering in the molecular layer. For example, Choi *et al.* have shown that electronic coupling for conjugated oligophenyleneimine (OPI) wire extends over 3 repeating units with ~100 nm red shift in the UV−vis absorption peak and then remains constant at 400 nm for longer OPI wires.[21] In the present case of FL, however, increasing layer thickness does not change the absorption spectrum and is a direct indication of weak electronic coupling between FL subunits. The large red-shift of the absorbance onset which occurs for all thicknesses of FL multilayer grafted on the surface compared to FL monomer in solution may have at least three origins: (i) electronic coupling between FL and the graphitic π system of the carbon electrode; (ii) intermolecular $\pi-\pi$ interactions in the FL layer; and (iii)

structural variations in FL−FL coupling within the molecular layer. At least over the thickness range examined, these effects do not produce an observable change in the UV−vis absorption spectrum with layer thickness. We conclude that a covalent bond between aromatic molecules is not enough to extend delocalization significantly beyond FL subunits in an oligomeric FL multilayer. The invariance of the UV−vis spectrum with thickness past a few nm clearly indicates weak electronic interactions between subunits and implies a localization length approximately equal to one or at most two FL molecules. Consideration of the molecular layer as a series of weakly interacting molecular orbitals is an important factor in controlling transport and is discussed in more detail below.

Structural Effects on Junction Behavior. To investigate effects of molecular structure on the electronic behavior observed for FL MJs, AQ and NAB films and devices were investigated and compared to BTB reported previously.[25] The UV−vis spectra of the FL, AQ, NAB, and BTB bonded to OTPPF are compared in Figure 5d after subtraction of the unmodified PPF spectrum, and Table 1 lists the optical gap and absorption onsets as well as DFT predictions. Notice that both the peak absorption and onset of absorption occur at significantly lower energy for BTB and NAB compared to AQ and FL. As shown in Figure 5c, the absorption onset for NAB bonded to OTPPF also shows a significant red shift compared to NAB monomer in solution, but the peak and onset wavelengths do not vary further with increasing thickness. Additional absorbance spectra for the four molecules are provided in Supporting Information section 4, and the salient results are summarized in Table 1.

Table 1. Orbital Energies, UV–vis Absorption and Current Densities

	FL	AQ	NAB	BTB
DFT LUMO[a] (eV)	−0.71	−2.76	−3.03	−1.48
DFT HOMO[a] (eV)	−5.75	−7.00	−6.66	−5.29
DFT H-L gap (eV)	5.04	4.24	3.63	3.81
TD-DFT peak[b] (eV)	4.71	5.12	3.49	3.52
UV–vis peak[b,c] (eV)	4.57	4.73	3.50	3.44
UV–vis onset[c] (eV)	3.18	3.12	1.93	1.93
J (8 nm)[d], A/cm^2, @ 0.5 V	2.2×10^{-6}	1.7×10^{-6}	6.1×10^{-5}	2.9×10^{-4}
J (10 nm)[d], A/cm^2 @ 0.5 V	–	2.1×10^{-8}	5.2×10^{-6}	1.2×10^{-4}

[a]For free molecule monomers *vs* vacuum reference, B3LYP 6-31G(d). [b]Major peak predicted for the free molecule in region of 200−700 nm. [c]Peak or onset for molecular multilayer bonded to OTPPF, after OTPFF spectrum subtracted. [d]Interpolated from attenuation plot of Figure 7a.

Molecular junctions were fabricated with the same PPF/molecule/eC/Au junction structure in all cases and d ranging from 3 to 13 nm. JV curves for the four molecules with similar thicknesses in the range of $d = 7.4−8.1$ nm are shown in Figure 6a, all exhibiting symmetry with bias and similar shape. However, J for BTB and NAB is much higher than that of FL and AQ, by a factor of ∼100 for $V = \pm 1$ V. Complete sets for AQ and NAB are provided in Supporting Information section 5 and Figures S9−S10. Plots of ln |J| *vs* $V^{1/2}$ for the same examples are shown in Figure 6b, showing linearity similar to FL ($R^2 = 0.9902−0.9992$ for all four cases) and large difference in J over the entire bias range. Complete sets of ln J *vs* $V^{1/2}$ curves for a range of thicknesses are provided in Figure S10 for AQ, NAB and BTB.

A statistically more valid comparison of the four molecules over a wide thickness range is the attenuation plot of Figure 7a, which incorporates data from ∼120 MJs with the PPF/molecule/eC/Au structure. Note that all four molecules have β values near 2.7 nm^{-1} for $d < 5$ nm and that FL and AQ are indistinguishable, with both equal β and equal J over the range of $d = 3.4−8.6$ nm. However, BTB and NAB depart significantly from the $\beta \sim 2.7$ nm^{-1} line when d exceeds 5 nm, resulting in very different attenuation slopes (*e.g.*, ∼ 1.0 nm^{-1} for BTB above 8 nm).[25] Note that for $d \sim 10$ nm, J for NAB at 0.5 V is >250 times greater than that for AQ, while J for BTB is >5000 times larger than that for AQ.

DISCUSSION

The experimental results demonstrate several unusual and in some cases unexpected aspects of transport in conjugated carbon-based molecular junctions. First, the exponential dependence of current on molecular layer thickness persists well beyond 5 nm, up to $d = 8.6$ nm for FL and $d = 10.6$ nm for AQ (Figure 7a). Second, linear ln J *vs* $V^{1/2}$ behavior was observed for all four molecules over a range of thicknesses, instead of the ln J *vs* V linearity expected for coherent tunneling (see Figure S10). Third, the optical gap of all four molecules is red-shifted upon bonding to PPF, particularly the onset of absorbance at long wavelengths. However, the UV−vis absorption spectrum is not further red-shifted with increasing thickness of molecular layers for all four molecules (Figure 5 and Supporting Information section 4). Fourth, the temperature dependence does not exhibit linear Arrhenius behavior anywhere between 200 and 440 K for the tested molecules, and the apparent activation energy decreases to <20 meV below ∼250 K. For AQ, FL, and BTB, ln J *vs* T is more linear (R^2 typically >0.94) than ln J *vs* $1/T$ (R^2 typically 0.80−0.89).

The results also show clear inconsistencies with transport mechanisms reported for other types of junction fabrication and molecular structures. The linearity of the attenuation plots for FL and AQ and the similarity of JV curve shapes over the 2−11 nm thickness range are not expected if the transport mechanism changes above 3−5 nm, as proposed for several other conjugated systems.[20−24] Furthermore, fitting the FL results to a Simmons tunneling model with both image charge and effective mass corrections ($m*/m_o = 0.3$, $\varepsilon = 6$)[13] requires a reduction of the barrier height from 2.2 eV for $d = 3.4$ nm to 0.75 eV for $d = 8.6$ nm to yield the observed currents. Such a reduction is physically unreasonable and is contradicted by the UV−vis absorption results, which show little change in absorption spectrum for both FL and AQ with layer thickness. Inspection of Figure 7c−d and Table 1 leads to serious inconsistencies with a "single level" model based on a tunneling barrier between the electrode Fermi level and either the molecular HOMO or LUMO. The PPF and e-carbon Fermi levels determined from Kelvin probe and ultraviolet photoelectron spectroscopy (UPS) are both −4.8 V *vs* vacuum.[41,42]
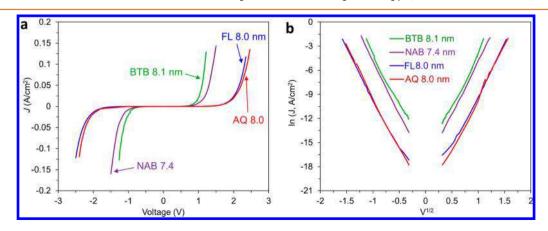

Figure 6. (a) JV curves of BTB, NAB, FL, and AQ with thicknesses close to 8 nm. (b) ln |J| *vs* $V^{1/2}$ plots for curves in panel a.
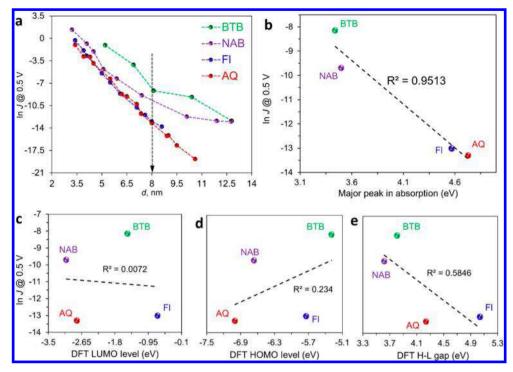
Figure 7. (a) Attenuation plots for BTB, NAB, FL, and AQ, all obtained at 0.5 V. (b) ln J for V = 0.5 V and d = 8 nm for the four molecules plotted *vs* the energy of the main UV−vis absorption peak of the molecular layer shown in Figure 4d. R^2 is the correlation coefficient for the linear fit shown. (c) The same ln J plotted *vs* the DFT determined LUMO energy of the free molecules (d) ln J *vs* free molecule HOMO energy from DFT. (e) ln J *vs* the DFT determined HOMO−LUMO gap.

From free molecule DFT energies, the HOMO or LUMO offsets for FL and AQ should differ by >2 eV (for LUMOs) or >1.2 eV (for HOMOs), which should result in a large difference in tunneling current due to the resulting changes in barrier height. However, Figure 7a shows that the current densities for FL and AQ are very similar over a 2−9 nm thickness range, and Figure 7c−d shows no correlation between the DFT HOMO and LUMO levels and the observed current density at V = 0.5 V when d ∼ 8 nm. These observations contradict a model assuming a tunneling barrier determined by the offsets of either the HOMO or LUMO relative to the electrode Fermi level. The similarity of transport for AQ and FL when d < 5 nm may be caused by strong coupling to the electrodes,[15,30,32] but only if such coupling extends up to and beyond 8 nm. Not only is this contradicted by the UV−vis results, but NAB and BTB do show significant departures from β-linearity for d > 5 nm. Although there is poor correlation of individual orbital energies with junction current, the HOMO−LUMO (H-L) gap correlates much better, determined either from the DFT energies (Figure 7e, R^2 = 0.585) or from the UV−vis absorption maxima of the molecular layer (Figure 7b, R^2 = 0.951). The junction current also correlates well (R^2 = 0.905) with the optical H-L gap predicted from TD-DFT for each of the four molecules, provided in Table 1. The consequences of this correlation are significant, in that the results imply that the H-L gap determines transport when d > 5 nm, rather than the relationship of either the HOMO or LUMO energies to the contact Fermi level.

A transport mechanism controlled by the H-L gap instead of the offset of either the HOMO or LUMO levels from the contact Fermi level is possible in carbon-based systems with some significant modifications to common models for transport in molecular junctions. First, suppose transport is "bulk" controlled rather than "interface" controlled. The strong electronic coupling between PPF and aromatic molecules and the linearity of the β plot over >8 nm imply that interfacial transport is *not* rate limiting. Provided interfacial "injection" of carriers is faster than transport in the film interior, the offsets between orbitals and the electrode Fermi levels should not affect the current density. Second, coherent tunneling may dominate transport only in a situation where the tunneling distance is not much greater than the localization length.[38] The absence of changes in the UV−vis spectra with thickness indicates limited delocalization within the molecular layer, since strong electronic coupling between molecules should decrease the optical gap for higher d. In the case of weak intermolecular interactions, transport might occur along a series of localized states, perhaps as small as a HOMO or LUMO orbital of individual molecules. Transport by a series of tunneling steps between localized states has been considered for several decades and is related to common mechanisms in disordered organic films, such as nearest-neighbor hopping (NNH) and variable range hopping (VRH).[43−47] Linearity of ln J with T instead of $1/T$ is predicted in the case of thermally assisted or multistep tunneling[43,48−50] and is consistent with the nearly linear ln J *vs* T behavior for FL MJs shown in Figure 4d and for BTB and AQ MJs shown in Figure S14.

The linearity of ln J with $V^{1/2}$ apparent in Figure 3 and 5b is expected for Poole−Frankel transport between "traps" or Schottky emission at interfaces, as noted above. A recent report on transport in molecular junctions containing iron-porphyrin multilayers with d > 10 nm concluded that the linear ln J *vs* $V^{1/2}$ behavior observed was due to Schottky emission at the electrode interfaces.[51] Both Poole−Frankel and Schottky include a field-dependent barrier height (ϕ), given by eq 1, where ϕ_0 is the barrier height at zero field, q is the elementary charge, ε the relative dielectric constant of the molecular layer,
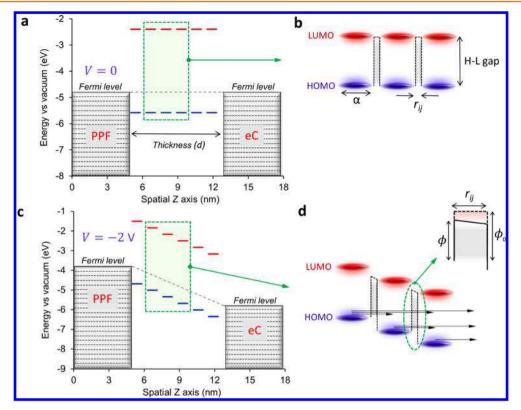
Figure 8. (a) Energy level diagram at zero bias for a FL junction with six pairs of localized HOMO and LUMO states, using free molecule DFT energies and a PPF Fermi level of −4.8 eV. (b) Magnification of three paired H-L states; α and r_{ij} are the localization length and tunneling distance between two neighboring states. (c) The same diagram as panel a for $V = -2$ V bias (PPF negative), assuming a linear potential profile through the molecular layer. (d) Magnification of panel c, with inset showing the tunneling barrier with height ϕ_0 at zero bias and ϕ with bias applied. Arrows indicate possible tunneling paths for electrons.

ε_0 the permittivity of free space, and V and d were defined previously:

$$\phi = \phi_0 - \left(\frac{q}{4d\pi\varepsilon\varepsilon_0}\right)^{1/2} V^{1/2} \quad (1)$$

Attempts to fit the Poole−Frankel or Schottky mechanisms to the observed JV curves for FL with varying thickness yielded physically unreasonable parameters, with barrier heights and dielectric constants that vary significantly with d (see Supporting Information, section 7). Poole−Frankel and Schottky emission should show Arrhenius temperature behavior with much stronger T dependence than any of the MJs reported here. However, the barrier height for sequential tunneling can also exhibit a dependence on electric field *via* eq 1, and thus yield ln J vs $V^{1/2}$ linearity, distinguished from Schottky or Poole−Frankel mechanisms by weak temperature dependence (linearity of *ln J* with T) and high thickness dependence.[48−50] Unlike the conclusion for Fe-porphyrin MJs,[51] transport in the carbon-based MJs studied here is controlled by "bulk" properties of the organic layer rather than "injection" at the interfaces. *In effect, transport barriers associated with the electrode/molecule interface become irrelevant to transport, provided electronic coupling at the interfaces is strong compared to that between localized states within the molecular layer interior.*

The schematic of Figure 8a depicts several elements of the proposed mechanism for multistep tunneling transport. Six pairs of HOMO and LUMO states represent the molecular layer, where each orbital may be localized on one or at most two FL molecules, with a localization length of α shown in

Figure 8b. These orbitals are broadened by disorder, electronic coupling, and vibrational states and are separated by a distance r_{ij}, resulting in a tunneling barrier with a height equal to the H-L gap and width equal to r_{ij}. Note that the orbital energies near the electrode interfaces are perturbed by electronic coupling with the contacts and may shift and broaden relative to the electrode Fermi level by partial charge transfer to the electrodes, often called a "vacuum level shift".[15,52−54] Provided "injection" of carriers is fast relative to bulk transport, the observed current is limited by tunneling through the H-L barrier, and tunneling may occur across more than one H-L gap (as shown in Figure 8d). In an applied electric field (Figure 8c−d), the barrier height is reduced, as shown in the inset of Figure 8d. Under this model, the important factors controlling the current density are the H-L gap in the "bulk" molecular layer, r_{ij}, α, and the number of steps required to transit across layer thickness d. The relative energies of the orbitals and the electrode Fermi level are not relevant to transport, since the rate-limiting step is tunneling across the H-L barrier within the molecular layer interior. A transport mechanism controlled by the molecular layer properties rather than the contacts, as we propose here, may be an advantage of aromatic carbon contacts such as sp^2 hybridized carbon or graphene. Several recent reports using carbon-based molecular junctions have identified attractive electronic properties and/or high stability when molecules are covalently bonded to carbon contacts.[41,55−57]

Finally, the current multistep tunneling model depends on "sites" separated by a barrier determined by the H-L gap in the film interior and assumes relatively rapid carrier transport at the carbon electrode interfaces due to strong electronic coupling

between the graphitic π system and the aromatic molecules. At the simplest limit, an electron moves from the HOMO of the molecule at an electrode interface into the electrode, thus creating a hole which is filled by tunneling from a nearby HOMO through the H-L barrier. Depending on the time scale, the hole could result in reorganization, leading to polaron formation and a mechanism similar to "polaron tunneling" proposed recently by Taherinia et al.[29] The small activation energies observed in the current devices, particularly at low T, are evidence against reorganization to a polaron being a prerequisite for transport and are more consistent with a multistep tunneling model such as that presented in Figure 8. Current research is focused on confirming the importance of the H-L gap to determine conductance in carbon-bases molecular junctions and investigating the generality of observation that carrier injection is not rate limiting.

CONCLUSIONS

Charge transport in aromatic carbon/molecule/carbon molecular junctions is strongly affected both by electronic coupling between the electrodes and the molecules and by relatively weak coupling between oligomer subunits. As a result, efficient transport does not correlate with the energies of molecular orbitals relative to the electrode Fermi levels, but is directly controlled by the HOMO−LUMO energy gap in the molecular layer interior. The factors of >1000 differences in conductance with variations in molecular structure observed for $d = 10$ nm result from changes in the H-L gap indicated directly by UV−vis absorption of molecular layers bonded to graphitic carbon. The unusual linearity of ln J with $V^{1/2}$ observed for all four molecules is consistent with lowering of the H-L tunneling barrier in the applied electric field, and the weak temperature dependence is expected for a multistep, sequential tunneling mechanism. The important parameters controlling electron transport are the H-L energy gap within the molecular layer, the tunneling distance between molecular orbitals (r_{ji}), the localization length (α), and the number of steps required to traverse the molecular layer. At least for the case of strong electronic coupling between carbon electrodes and aromatic molecular layers, the findings provide useful guidance for rational design of molecular electronic devices with desired electronic behaviors.

METHODS

Fabrication of junctions on pyrolyzed photoresist film (PPF) was conducted as described previously, with electron-beam deposited carbon (eC) and Au top contacts.[19,25] Junctions are designated with subscripts in nm on the "stack" of contacts and molecular layers, viz. PPF/FL$_{5.0}$/eC$_{10}$/Au$_{20}$ (FL$_{5.0}$ designates a FL oligomer with $d = 5.0$ nm). The same junction structure was used in all cases, with variation only of the identity and thickness of the molecular layer, and the junction area was 0.00125 cm^2 (250 × 500 μm). FL deposition by reduction of diazonium reagents is radical-mediated, hence the films are covalently bonded to the PPF and between FL subunits, with partial ordering along the axis perpendicular to the PPF. The thickness of the molecular layer was controlled by the scan range of the electrochemical reduction using the conditions listed in Supporting Information section 1 and was validated by AFM "scratching."[58] All electrical measurements were done with a Keithley 2602 source-meter in 4-wire configuration and custom program to have dynamic NPLC over a wide range of applied voltage bias. Additional experimental details regarding fabrication and electrical measurements are provided in Supporting Information sections 1 and 2.

ASSOCIATED CONTENT

Ⓢ Supporting Information

The Supporting Information is available free of charge on the ACS Publications website at DOI: 10.1021/acsnano.7b00597.

Junction fabrication details, absorption spectra, temperature results, and additional JV curves and statistics (PDF)

AUTHOR INFORMATION

Corresponding Author
*E-mail: richard.mccreery@ualberta.ca.

ORCID Ⓘ
Amin Morteza Najarian: 0000-0002-0455-0451
Richard L. McCreery: 0000-0002-1320-4331

Notes
The authors declare no competing financial interest.

REFERENCES

(1) Su, T. A.; Neupane, M.; Steigerwald, M. L.; Venkataraman, L.; Nuckolls, C. Chemical Principles of Single-Molecule Electronics. *Nat. Rev. Mater.* **2016**, *1*, 16002.

(2) Metzger, R. M. Unimolecular Electronics. *Chem. Rev.* **2015**, *115*, 5056−5115.

(3) Xiang, D.; Wang, X.; Jia, C.; Lee, T.; Guo, X. Molecular-Scale Electronics: From Concept to Function. *Chem. Rev.* **2016**, *116*, 4318−4440.

(4) McCreery, R.; Yan, H.; Bergren, A. J. A Critical Perspective on Molecular Electronic Junctions: There is Plenty of Room in the Middle. *Phys. Chem. Chem. Phys.* **2013**, *15*, 1065−1081.

(5) Moth-Poulsen, K.; Bjornholm, T. Molecular Electronics With Single Molecules in Solid-State Devices. *Nat. Nanotechnol.* **2009**, *4*, 551−556.

(6) McCreery, R. L. The Merger of Electrochemistry and Molecular Electronics. *Chem. Rec.* **2012**, *12*, 149−163.

(7) Reus, W. F.; Nijhuis, C. A.; Barber, J. R.; Thuo, M. M.; Tricard, S.; Whitesides, G. M. Statistical Tools for Analyzing Measurements of Charge Transport. *J. Phys. Chem. C* **2012**, *116*, 6714−6733.

(8) Chiechi, R. C.; Weiss, E. A.; Dickey, M. D.; Whitesides, G. M. Eutectic Gallium-Indium (EGaIn): A Moldable Liquid Metal for Electrical Characterization of Self-Assembled Monolayers. *Angew. Chem., Int. Ed.* **2008**, *47*, 142−144.

(9) Akkerman, H. B.; Blom, P. W. M.; de Leeuw, D. M.; de Boer, B. Towards Molecular Electronics with Large-Area Molecular Junctions. *Nature* **2006**, *441*, 69.

(10) Bonifas, A. P.; McCreery, R. L. "Soft" Au, Pt and Cu Contacts for Molecular Junctions Through Surface-Diffusion-Mediated Deposition. *Nat. Nanotechnol.* **2010**, *5*, 612−617.

(11) Finklea, H. O., Electrochemistry of Organized Monolayers of Thiols and Related Molecules on Electrodes. In *Electroanalytical Chemistry*; Bard, A. J., Ed.; Dekker: New York, 1996; Vol. 19, pp 109−335.

(12) Creager, S.; Yu, C. J.; Bamdad, C.; O'Connor, S.; MacLean, T.; Lam, E.; Chong, Y.; Olsen, G. T.; Luo, J.; Gozin, M.; Kayyem, J. F. Electron Transfer at Electrodes through Conjugated "Molecular Wire" Bridges. *J. Am. Chem. Soc.* **1999**, *121*, 1059−1064.

(13) Bergren, A. J.; McCreery, R. L.; Stoyanov, S. R.; Gusarov, S.; Kovalenko, A. Electronic Characteristics and Charge Transport Mechanisms for Large Area Aromatic Molecular Junctions. *J. Phys. Chem. C* **2010**, *114*, 15806−15815.

(14) He, J.; Chen, F.; Li, J.; Sankey, O.; Terazono, Y.; Herroro, C.; Gust, D.; Moore, T.; Moore, A. L.; Lindsay, S. M. Electronic Decay Constant of Carotenoid Polyenes From Single-Molecule Measurements. *J. Am. Chem. Soc.* **2005**, *127*, 1384−1385.

(15) Sayed, S. Y.; Fereiro, J. A.; Yan, H.; McCreery, R. L.; Bergren, A. J. Charge Transport in Molecular Electronic Junctions: Compression of the Molecular Tunnel Barrier in the Strong Coupling Regime. *Proc. Natl. Acad. Sci. U. S. A.* **2012**, *109*, 11498−11503.

(16) Sedghi, G.; Esdaile, L. J.; Anderson, H. L.; Martin, S.; Bethell, D.; Higgins, S. J.; Nichols, R. J. Comparison of the Conductance of Three Types of Porphyrin-Based Molecular Wires: β,meso,β-Fused Tapes, meso-Butadiyne-Linked and Twisted meso-meso Linked Oligomers. *Adv. Mater.* **2012**, *24*, 653−657.

(17) Sedghi, G.; Garcia-Suarez, V. M.; Esdaile, L. J.; Anderson, H. L.; Lambert, C. J.; Martin, S.; Bethell, D.; Higgins, S. J.; Elliott, M.; Bennett, N.; Macdonald, J. E.; Nichols, R. J. Long-Range Electron Tunnelling in Oligo-Porphyrin Molecular Wires. *Nat. Nanotechnol.* **2011**, *6*, 517−523.

(18) Tuccitto, N.; Ferri, V.; Cavazzini, M.; Quici, S.; Zhavnerko, G.; Licciardello, A.; Rampi, M. A. Highly Conductive 40-nm-long Molecular Wires Assembled by Stepwise Incorporation of Metal Centres. *Nat. Mater.* **2009**, *8*, 41−46.

(19) Yan, H.; Bergren, A. J.; McCreery, R. L. All-Carbon Molecular Tunnel Junctions. *J. Am. Chem. Soc.* **2011**, *133*, 19168−19177.

(20) Luo, L.; Choi, S. H.; Frisbie, C. D. Probing Hopping Conduction in Conjugated Molecular Wires Connected to Metal Electrode. *Chem. Mater.* **2011**, *23*, 631−645.

(21) Choi, S. H.; Kim, B.; Frisbie, C. D. Electrical Resistance of Long Conjugated Molecular Wires. *Science* **2008**, *320*, 1482−1486.

(22) Lu, Q.; Liu, K.; Zhang, H.; Du, Z.; Wang, X.; Wang, F. From Tunneling to Hopping: A Comprehensive Investigation of Charge Transport Mechanism in Molecular Junctions Based on Oligo(p-phenylene ethynylene)s. *ACS Nano* **2009**, *3*, 3861−3868.

(23) Amdursky, N.; Marchak, D.; Sepunaru, L.; Pecht, I.; Sheves, M.; Cahen, D. Electronic Transport *via* Proteins. *Adv. Mater.* **2014**, *26*, 7142−7161.

(24) Lee, S. K.; Yamada, R.; Tanaka, S.; Chang, G. S.; Asai, Y.; Tada, H. Universal Temperature Crossover Behavior of Electrical Conductance in a Single Oligothiophene Molecular Wire. *ACS Nano* **2012**, *6*, 5078−5082.

(25) Yan, H.; Bergren, A. J.; McCreery, R.; Della Rocca, M. L.; Martin, P.; Lafarge, P.; Lacroix, J. C. Activationless Charge Transport Across 4.5 to 22 nm in Molecular Electronic Junctions. *Proc. Natl. Acad. Sci. U. S. A.* **2013**, *110*, 5326−5330.

(26) Xie, Z.; Bâldea, I.; Smith, C. E.; Wu, Y.; Frisbie, C. D. Experimental and Theoretical Analysis of Nanotransport in Oligophenylene Dithiol Junctions as a Function of Molecular Length and Contact Work Function. *ACS Nano* **2015**, *9*, 8022−8036.

(27) Baldea, I.; Xie, Z.; Frisbie, C. D. Uncovering a Law of Corresponding States for Electron Tunneling in Molecular Junctions. *Nanoscale* **2015**, *7*, 10465−10471.

(28) Luo, L.; Balhorn, L.; Vlaisavljevich, B.; Ma, D.; Gagliardi, L.; Frisbie, C. D. Hopping Transport and Rectifying Behavior in Long Donor−Acceptor Molecular Wires. *J. Phys. Chem. C* **2014**, *118*, 26485−26497.

(29) Taherinia, D.; Smith, C. E.; Ghosh, S.; Odoh, S. O.; Balhorn, L.; Gagliardi, L.; Cramer, C. J.; Frisbie, C. D. Charge Transport in 4 nm Molecular Wires with Interrupted Conjugation: Combined Experimental and Computational Evidence for Thermally Assisted Polaron Tunneling. *ACS Nano* **2016**, *10*, 4372−4383.

(30) Kondratenko, M.; Stoyanov, S. R.; Gusarov, S.; Kovalenko, A.; McCreery, R. L. Theoretical Modeling of Tunneling Barriers in Carbon-Based Molecular Electronic Junctions. *J. Phys. Chem. C* **2015**, *119*, 11286−11295.

(31) McCreery, R. L. Effects of Electronic Coupling and Electrostatic Potential on Charge Transport in Carbon-Based Molecular Electronic Junctions. *Beilstein J. Nanotechnol.* **2016**, *7*, 32−46.

(32) Gibbs, J.; Otero de la Roza, A.; Bergren, A. J.; DiLabio, G. A. Interpretation of Molecular Device Transport Calculation. *Can. J. Chem.* **2016**, *94*, 1022−1027.

(33) Sze, S. M. *Physics of Semiconductor Devices*, 2nd ed; Wiley: New York, 1981.

(34) Ivashenko, O.; Bergren, A. J.; McCreery, R. L. Monitoring of Energy Conservation and Losses in Molecular Junctions Through Characterization of Light Emission. *Adv. Electron. Mater.* **2016**, *2*, 1600351.

(35) Donner, S.; Li, H. W.; Yeung, E. S.; Porter, M. D. Fabrication of Optically Transparent Carbon Electrodes by the Pyrolysis of Photoresist Films: Approach to Single-Molecule Spectroelectrochemistry. *Anal. Chem.* **2006**, *78*, 2816−2822.

(36) Tian, H.; Bergren, A. J.; McCreery, R. L. UltravioletVisible Spectroelectrochemistry of Chemisorbed Molecular Layers on Optically Transparent Carbon Electrodes. *Appl. Spectrosc.* **2007**, *61*, 1246−1253.

(37) Fereiro, J. A.; Kondratenko, M.; Bergren, A. J.; McCreery, R. L. Internal Photoemission in Molecular Junctions: Parameters for Interfacial Barrier Determinations. *J. Am. Chem. Soc.* **2015**, *137*, 1296−1304.

(38) Ortiz, R. P.; Facchetti, A.; Marks, T. J. High-k Organic, Inorganic, and Hybrid Dielectrics for Low-Voltage Organic Field-Effect Transistors. *Chem. Rev.* **2010**, *110*, 205−239.

(39) Tsuda, A.; Osuka, A. Fully Conjugated Porphyrin Tapes with Electronic Absorption Bands That Reach into Infrared. *Science* **2001**, *293*, 79−82.

(40) Choi, S. H.; Risko, C.; Delgado, M. C. R.; Kim, B.; Bredas, J.-L.; Frisbie, C. D. Transition from Tunneling to Hopping Transport in Long, Conjugated Oligo-imine Wires Connected to Metals. *J. Am. Chem. Soc.* **2010**, *132*, 4358−4368.

(41) Morteza Najarian, A.; Szeto, B.; Tefashe, U. M.; McCreery, R. L. Robust All-Carbon Molecular Junctions on Flexible or Semi-Transparent Substrates Using "Process-Friendly" Fabrication. *ACS Nano* **2016**, *10*, 8918−8928.

(42) Yan, H.; McCreery, R. L. Anomalous Tunneling in Carbon/Alkane/TiO2/Gold Molecular Electronic Junctions: Energy Level Alignment at the Metal/Semiconductor Interface. *ACS Appl. Mater. Interfaces* **2009**, *1*, 443−451.

(43) Roberts, G. G.; Apsley, N.; Munn, R. W. Temperature Dependent Electronic Conduction in Semiconductors. *Phys. Rep.* **1980**, *60*, 59−150.

(44) Stallinga, P. Electronic Transport in Organic Materials: Comparison of Band Theory with Percolation/(Variable Range) Hopping Theory. *Adv. Mater.* **2011**, *23*, 3356−3362.

(45) Tessler, N.; Preezant, Y.; Rappaport, N.; Roichman, Y. Charge Transport in Disordered Organic Materials and Its Relevance to Thin-Film Devices: A Tutorial Review. *Adv. Mater.* **2009**, *21*, 2741−2761.

(46) Lee, P. A.; Ramakrishnan, T. Disordered Electronic Systems. *Rev. Mod. Phys.* **1985**, *57*, 287.

(47) Baranovskii, S.; Rubel, O., Charge Transport in Disordered Materials. In *Springer Handbook of Electronic and Photonic Materials*; Springer: New York, 2006; pp 161−186.

(48) Roberts, G. G.; Polanco, J. I. Thermally Assisted Tunnelling in Dielectric Films. *phys. status solidi A* **1970**, *1*, 409−420.

(49) Riben, A. R.; Feucht, D. L. Electrical Transport in nGe-pGaAs Heterojunctions. *Int. J. Electron.* **1966**, *20*, 583−599.

(50) Martinuzzi, S.; Mallem, O. Dark-Current Conduction Processes in CdS−Cu2S Thin-Film Photocells. *phys. status solidi A* **1973**, *16*, 339−344.

(51) Karipidou, Z.; Branchi, B.; Sarpasan, M.; Knorr, N.; Rodin, V.; Friederich, P.; Neumann, T.; Meded, V.; Rosselli, S.; Nelles, G.; Wenzel, W.; Rampi, M. A.; von Wrochem, F. Ultrarobust Thin-Film Devices from Self-Assembled Metal−Terpyridine Oligomers. *Adv. Mater.* **2016**, *28*, 3473−3480.

(52) Braun, S.; Salaneck, W. R.; Fahlman, M. Energy-Level Alignment at Organic/Metal and Organic/Organic Interfaces. *Adv. Mater.* **2009**, *21*, 1450−1472.

(53) Hwang, J.; Wan, A.; Kahn, A. Energetics of Metal−Organic Interfaces: New Experiments and Assessment of the Field. *Mater. Sci. Eng., R* **2009**, *64*, 1−31.

(54) Vilan, A.; Yaffe, O.; Biller, A.; Salomon, A.; Kahn, A.; Cahen, D. Molecules on Si: Electronics with Chemistry. *Adv. Mater.* **2010**, *22*, 140−159.

(55) Jia, C.; Migliore, A.; Xin, N.; Huang, S.; Wang, J.; Yang, Q.; Wang, S.; Chen, H.; Wang, D.; Feng, B.; Liu, Z.; Zhang, G.; Qu, D.-H.; Tian, H.; Ratner, M. A.; Xu, H. Q.; Nitzan, A.; Guo, X. Covalently Bonded Single-Molecule Junctions With Stable and Reversible Photoswitched Conductivity. *Science* **2016**, *352*, 1443−1445.

(56) Jia, C.; Ma, B.; Xin, N.; Guo, X. Carbon Electrode−Molecule Junctions: A Reliable Platform for Molecular Electronics. *Acc. Chem. Res.* **2015**, *48*, 2565−2575.

(57) Kim, D.; Jeong, H.; Lee, H.; Hwang, W.-T. T.; Wolf, J.; Scheer, E.; Huhn, T.; Jeong, H.; Lee, T. Flexible Molecular-Scale Electronic Devices Composed of Diarylethene Photoswitching Molecules. *Adv. Mater.* **2014**, *26*, 3968−3973.

(58) Anariba, F.; DuVall, S. H.; McCreery, R. L. Mono- and Multilayer Formation by Diazonium Reduction on Carbon Surfaces Monitored with Atomic Force Microscopy ″Scratching″. *Anal. Chem.* **2003**, *75*, 3837−3844.